PROBING THE QCD PHASE DIAGRAM WITH DILEPTONS — A STUDY USING COARSE-GRAINED TRANSPORT DYNAMICS*

Stephan Endres, Hendrik van Hees, Marcus Bleicher

Frankfurt Institute for Advanced Studies
Ruth-Moufang-Strasse 1, 60438 Frankfurt am Main, Germany
and
Institut für Theoretische Physik, Universität Frankfurt
Max-von-Laue-Strasse 1, 60438 Frankfurt am Main, Germany

(Received February 16, 2017)

Dilepton production in heavy-ion collisions at various energies is studied using coarse-grained transport simulations. Microscopic output from the Ultra-relativistic Quantum Molecular Dynamics (UrQMD) model is hereby put on a grid of space-time cells which allows to extract the local temperature and chemical potential in each cell via an equation of state. The dilepton emission is then calculated applying in-medium spectral functions from hadronic many-body theory and partonic production rates based on lattice calculations. The comparison of the resulting spectra with experimental data shows that the dilepton excess beyond the decay contributions from a hadronic cocktail reflects the trajectory of the fireball in the T–μ_{B} plane of the QCD phase diagram.

DOI:10.5506/APhysPolBSupp.10.549

1. Introduction

Lepton pairs represent excellent probes for the properties of hot and dense matter created in heavy-ion collisions. Their cross section for interactions is extremely small so that they leave the produced fireball unscathed. In addition, dileptons directly couple to the vector current and, therefore, give access to the corresponding iso-scalar and iso-vector spectral functions, which allows one to learn about: *(i)* the properties of hadrons in the medium, *(ii)* the predicted deconfinement and *(iii)* chiral symmetry restoration [1].

* Presented at the "Critical Point and Onset of Deconfinement" Conference, Wrocław, Poland, May 30–June 4, 2016.

However, the interpretation of experimental dilepton spectra is challenging. Our understanding of the strong interaction, the properties of matter and — in consequence — the processes driving the dynamics in a heavy-ion collision is still limited. Because a full solution of QCD from first principles is not possible yet, theory has to rely on the use of models. Basically, there exist two different approaches for the description of heavy-ion collisions, and both have some advantages and disadvantages: While in macroscopic models such as fireball parameterizations or hydrodynamics the implementation of medium effects is straightforward, they require a short mean free path of the hadrons; in consequence, they are only applicable at sufficiently high collision energies and only for the hot and dense stage of the reaction. On the other hand, microscopic transport approaches account for the individual hadron–hadron interactions at all stages of the collision, but effects of finite temperature and density as, *e.g.*, spectral modifications or phase transitions are difficult to implement.

One option to further improve the theoretical description is to implement effective solutions for the full non-equilibrium quantum transport problem [2]. However, this is an extremely difficult task which requires full self-consistency. The second path is to connect the microscopic and macroscopic descriptions and combine the advantages of both pictures. Following the latter idea, the goal of the present work is to fully determine the macroscopic evolution from an underlying microscopic picture.

2. Coarse-graining approach

Based on the previous work by Huovinen and collaborators [3], the coarse-graining approach strongly simplifies the description obtained from the microscopic dynamics by reducing the information to a few thermodynamic quantities. As only a summarizing sketch of the approach can be given here, we refer for further details to Ref. [4].

In general, the model can be subdivided into three steps as follows:

1. A large ensemble of events is calculated with the UrQMD transport model [5], which describes the positions and momenta of all hadrons in the system for each time-step. A sufficient number of events is necessary to obtain a smooth distribution function $f(x, p, t)$. The output is then put on a space-time grid of small cells, which allows to determine the local baryon four-flow j^{μ}_{B} and the energy-momentum tensor $T^{\mu\nu}$. Applying Eckart's requirement of vanishing baryon flow, one can define the rest-frame for each cell and determine the local energy and baryon density, ε and ρ_{B}.

2. To obtain the temperature T and chemical potential μ_B in each cell, an equation of state (EoS) is required, which relates the thermodynamic quantities to the local densities ε and ρ_B. We use here *(i)* a hadron-gas EoS [6] for $T \leq 170\,\mathrm{MeV}$ and *(ii)* an EoS fitted to lattice calculations [7] for higher temperatures. While the hadron-gas EoS provides good consistency with the underlying microscopic dynamics because it includes the same degrees of freedom as the UrQMD model, the lattice EoS is necessary for a correct description of the deconfined phase above the critical temperature. To account for deviations from chemical equilibrium, also the local pion chemical potential is extracted.

3. With given T and μ_B, one can calculate the thermal dilepton emission for each cell. In a system in equilibrium, the production rate is determined by the imaginary part of the electromagnetic current–current correlator $\Pi^{(\mathrm{ret})}$, which is (in the hadronic phase) related to the spectral distributions of the light vector mesons up to $M = 1\,\mathrm{GeV}/c^2$, according to the current-field identity. To include medium effects, we use state-of-the-art spectral functions for the ρ and ω meson from hadronic many-body theory [8]. At higher masses, $\Pi^{(\mathrm{ret})}$ is dominated by a continuum of multi-meson states, for which the rates are obtained using a chiral-reduction approach [9]. In the QGP phase, the main contribution to the dilepton production is given by quark–antiquark annihilation. Here, we apply thermal emission rates obtained from lattice calculations [10].

3. Summary of results

Dilepton production from SIS 18 up to the LHC energies has been studied in detail with the coarse-graining approach; the corresponding results (compared to experimental data) can be found in Ref. [4]. They show that, at all energies, the measured dilepton excess over the hadronic decay cocktail can be interpreted as an effect of medium-modified spectral distributions, reflecting the emission conditions. In these proceedings, we focus on the connection between the trajectory of the fireball in the QCD phase diagram and the resulting dilepton spectra.

In Fig. 1, the thermal hadronic dilepton yield for central Au+Au collisions in relation to the value of μ_B at the source (*i.e.*, in the emitting cell) is shown for different collision energies from FAIR to RHIC. Within this energy range, one observes a strong variation of the baryochemical potential: While for $E_{\mathrm{lab}} = 2\,A\mathrm{GeV}$, one finds a clear peak of the thermal dilepton emission for $\mu_B = 0.7$–$0.9\,\mathrm{GeV}$, most lepton pairs at RHIC stem from cells with (nearly) vanishing baryochemical potential. Consequently,

strong baryonic effects on the spectral shapes of the vector mesons can be expected for low FAIR energies, while their influence gradually decreases when going to higher collision energies. At the same time, the temperature increases from a maximum value of $T \approx 100\,\mathrm{MeV}$ at the lower FAIR energies up to 400–500 MeV for $\sqrt{s} = 200\,A\mathrm{GeV}$ at RHIC (not shown here).

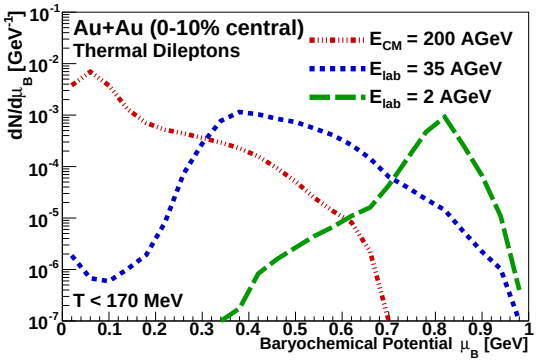

Fig. 1. Thermal dilepton emission in dependence on μ_B. The results are shown for central Au+Au collisions at the FAIR energies $E_\mathrm{lab} = 2$ and 35 AGeV as well as for the top RHIC energy $\sqrt{s} = 200\,A\mathrm{GeV}$. Only the hadronic emission, *i.e.*, the yield for $T < 170\,\mathrm{MeV}$, is considered.

How do the thermodynamic properties of the fireball show up in the dilepton spectra? The corresponding thermal invariant-mass yields are presented in Fig. 2. For the lowest collision energy $E_\mathrm{lab} = 2\,A\mathrm{GeV}$, the influence of the large μ_B is obvious; the spectrum shows a significant enhancement at low masses resulting in a Dalitz-like shape. This is caused by the strong

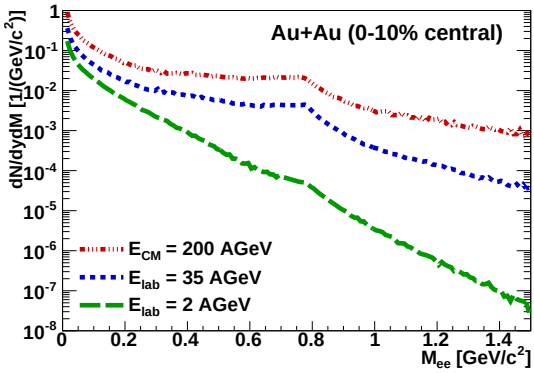

Fig. 2. Thermal dilepton invariant mass spectra $\mathrm{d}N/(\mathrm{d}y\,\mathrm{d}M)$ for central Au+Au collisions and the same energies as considered in Fig. 1. The results show the yield at mid-rapidity, $|y_\mathrm{ee}| < 0.5$.

coupling of the ρ meson to the baryonic Δ and N^*_{1520} resonances. For the top FAIR energy $E_{\rm lab} = 35\,A$GeV, the spectrum is much flatter due to decreasing baryonic influence and higher temperatures. Especially, the increase of T results in a larger contribution at higher masses. This trend continues for the top RHIC energy. However, the shape of the spectrum shows only a small qualitative change, although the fraction of partonic emission from the QGP increases strongly between FAIR and RHIC energies. The present results indicate that the thermal emission rates from hadronic and partonic matter are dual to a large extent, resulting in a conformable spectral shape. Thus, the identification of signals for a phase transition in the spectra requires systematic and precise studies, which remains a challenge for the future experiments at FAIR and the beam-energy scan program at RHIC.

The authors acknowledge Ralf Rapp for providing the parameterization of the spectral functions. This work was supported by the BMBF, HIC for FAIR, and H-QM.

REFERENCES

[1] R. Rapp, J. Wambach, *Adv. Nucl. Phys.* **25**, 1 (2000).

[2] L.P. Kadanoff, G. Baym, *Quantum Statistical Mechanics: Green's Function Methods in Equilibrium and Non-Equilibrium Problems*, W.A. Benjamin, New York 1962.

[3] P. Huovinen, M. Belkacem, P.J. Ellis, J.I. Kapusta, *Phys. Rev. C* **66**, 014903 (2002).

[4] S. Endres, H. van Hees, J. Weil, M. Bleicher, *Phys. Rev. C* **91**, 054911 (2015); **92**, 014911 (2015); S. Endres, H. van Hees, M. Bleicher, *Phys. Rev. C* **93**, 054901 (2016); **94**, 024912 (2016).

[5] S.A. Bass *et al.*, *Prog. Part. Nucl. Phys.* **41**, 255 (1998); M. Bleicher *et al.*, *J. Phys. G* **25**, 1859 (1999).

[6] D. Zschiesche *et al.*, *Phys. Lett. B* **547**, 7 (2002).

[7] M. He, R.J. Fries, R. Rapp, *Phys. Rev. C* **85**, 044911 (2012).

[8] R. Rapp, J. Wambach, *Eur. Phys. J. A* **6**, 415 (1999).

[9] H. van Hees, R. Rapp, *Nucl. Phys. A* **806**, 339 (2008).

[10] H.-T. Ding *et al.*, *Phys. Rev. D* **83**, 034504 (2011).